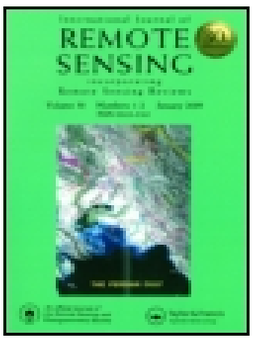

International Journal of Remote Sensing

ISSN: 0143-1161 (Print) 1366-5901 (Online) Journal homepage: http://www.tandfonline.com/loi/tres20

Mapping urban land surface temperature using remote sensing techniques and artificial neural network modelling

Nawras Shatnawi & Hani Abu Qdais

To cite this article: Nawras Shatnawi & Hani Abu Qdais (2019): Mapping urban land surface temperature using remote sensing techniques and artificial neural network modelling, International Journal of Remote Sensing, DOI: 10.1080/01431161.2018.1557792

To link to this article: https://doi.org/10.1080/01431161.2018.1557792

Published online: 15 Jan 2019.

INTERNATIONAL JOURNAL OF REMOTE SENSING
https://doi.org/10.1080/01431161.2018.1557792

Taylor & Francis
Taylor & Francis Group

Mapping urban land surface temperature using remote sensing techniques and artificial neural network modelling

Nawras Shatnawi [a] and Hani Abu Qdais[b]

[a]Surveying and Geomatics Engineering Department, Al-Balqa Applied University, Al-Salt, Jordan; [b]Civil Engineering Department, Jordan University of Science and Technology, Irbid, Jordan

ABSTRACT

The objective of the present study is to monitor and predict the changes in land surface temperature (LST) in the North of Jordan during the Period 2000 to 2016. Due to political instability in the nearby countries Syria and Iraq, Jordan has witnessed increased influxes of refugees, starting from the year 2003, which has been led to the urban expansion in the area that reflected on the climatic conditions and affected the LST values. Satellite images were used for providing LST, the acquired images represented two seasons of each year, namely summer and winter. Simulation and prediction of LST values for the next 10 years were carried out using nonlinear autoregressive exogenous (NARX) artificial neural network (ANN) model. The inputs to the model consist of meteorological data collected from eight stations in the study area, population, and land use and land cover (LULC). In fact, LULC was expressed in terms of normalized difference building index (NDBI) and normalized difference vegetation index (NDVI) that were obtained from satellite images. The model showed a high correlation between these parameters and the values of simulated LST, where the correlation coefficient for the training set, validation set, testing set and for the entire data ranged from 0.91 to 0.92. Based on the predicted LST values, LST maps for the next 10 years were developed and compared with the present actual LST maps for the year 2016. The comparison has shown an average increase of 1.1 °C in the average LST values, which is considered a significant increase compared with previous studies.

ARTICLE HISTORY
Received 31 December 2017
Accepted 18 November 2018

1. Introduction

Urbanization is a major complex process of converting rural lifestyles into urban which induced by the movement of the population from rural to urban areas. It can be defined as the changes that occur in the territorial and socio-economic progress of an area, including the general transformation of land use categories from being non-developed to developed (Weber 2001). Currently, almost half of the world's population live in urban areas and it is expected to reach 60% of the world's population by the year 2030. Furthermore, the number of megacities will reach 100 by 2025 (Avelar, Zah, and Tavares-Corrêa 2009). Urbanization and growth go

CONTACT Nawras Shatnawi nnshatnawi@bau.edu.jo Surveying and Geomatics Engineering Department, Al-Balqa Applied University, Al-Salt 19117, Jordan

hand in hand, as urbanization is essential for socio-economic transformation, wealth generation, prosperity and development (UN-Habitat 2016). The increasing trend in global urbanization induced many researchers to investigate the potential impacts of man-made activities on urban thermal environment such as the land surface temperature (LST) and urban heat island effect (UHI) (Ahmed et al. 2013), as urban centres experience higher temperatures than surrounding suburban and rural areas (Bhargava, Lakmini, and Bhargava 2017).

Jordan is one of the countries in the Middle East that witnessed in the last decade a rapid expansion of the urban areas because of the increased influxes of the refugees from the nearby countries. The population of Jordan has increased noticeably from 2010 to 2017 (DOS, 2017). According to the United Nations High Council for Refugees (UNHCR), the number of registered Syrian refugees is about 654,582, while the actual number of registered and non-registered refugees is assumed to be much higher (UNHCR, 2017).

Due to the political and military conflicts in the nearby countries of Syria and Iraq, in the recent years Jordan has witnessed high influxes of refugees from Iraq in 2003, and from Syria in 2011. The number of Iraqi refugees in the year 2003 has increased the population of Jordan by 18%. On the other hand, the Jordanian government estimates that around 1.3 million Syrians are living in Jordan, including both unregistered refugees and Syrians who had been living there before the war (UNHCR 2014). The current study covers the Northern part of Jordan where 80% of the Syrian refugees had settled. For example, as a result of the Syrian refugee's influxes, in Mafraq governorate the population has increased by 100% (UNHCR 2014). All of the

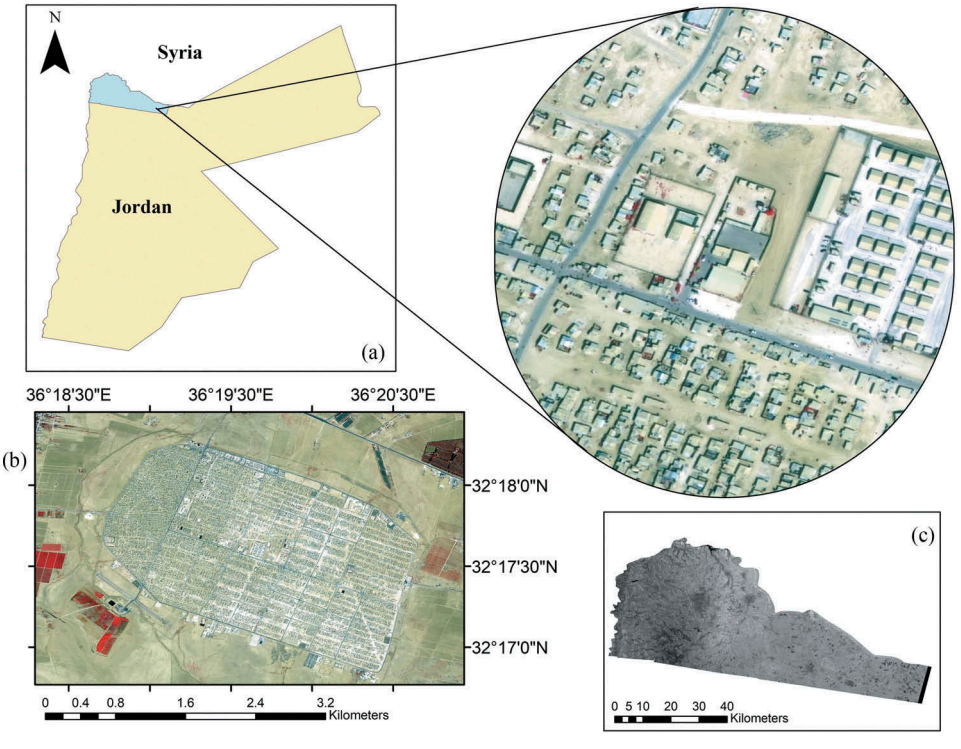

Figure 1. (a). Location of Al Za'atari refugees camp in the north of Jordan, (b). GeoEye satellite image. A 0.5 m spatial resolution, April 2016), (c). Original LANDSAT image of used Thermal Band.

sudden, one of the biggest refugees' camps in the world (Al Zaattari camp) has emerged in the desert of Mafraq as a small town, as shown in Figure 1. Refugees' influxes plus the natural population growth have resulted in rapid expansion of the urban areas and reshaping of the Jordanian urban landscape (World Bank 2017). Such changes are usually affecting the LST (Feizizadeh et al., 2013).

The rapid population growth in Jordan together with the high rate of urbanization, industrialization and increase in the number of transportation vehicles have adversely affected the situation in the urban environment. This has been reflected on the over-exploitation of many of its natural resources and consequently resulted in several environmental problems such as air pollution and higher temperature (Hadadin and Tarawneh 2007, Makhamreh and Almanasyeha 2011). UHI effects are due to meteorological and urbanization factors that increase urban temperature and the corresponding electricity demand in an urban area (Shahmohamadi et al. 2010). Oke et al. (1991) has correlated UHI intensity to the size of the urban population and found a direct relationship between the two parameters, where an increase in population leads to increased in UHI intensity. Emmanuel (2005) showed that the UHI is the accumulated warm air over the high density of built-up areas. Asimakopoulos, Assimakopoulos, and Chrisomallidou (2001) stated that the constructions in urban areas absorb heat during the day and re-emit it after sunset, creating high-temperature differences between urban and rural areas. According to (Bhargava, Lakmini, and Bhargava 2017), there are various causes for the formation of the UHI in the cities which include the high fraction of built-up areas that composed of buildings and pavements with less vegetative cover.

Air temperature is a key variable in a wide range of environmental applications including vector-borne disease bionomics (Kuhn, Campbell-Lendrum, and Davies 2002), terrestrial hydrology (Chow, Maidment, and Mays 1988), biosphere processes and climate change (Prince and Goward 1995). Although monitoring of the UHI is important, it is difficult to set up dense observation networks of air temperature. However, several studies investigated the usage of the (LST) derived from satellite images as an indicator of heat island (Zahng et al.,2008). LST is an important factor controlling most physical, chemical and biological process on Earth. Knowledge of LST is necessary for many environmental studies and management activities of the Earth's resources (Li and Becker 1993), many studies have shown a strong correlation between LST and air pollution (Al-Seroury 2012; Zheng et al. 2017). Moreover, the areas with low normalized difference vegetation index (NDVI), high built-up density, road density, and LST are consistent with high concentrations of pollutants. LST is a crucial climate parameter, and it is of great importance for analyzing the UHIs and local climate changes (Voogt and Oke 2003, Kaya et al. 2012).

Meteorological measurements provide accurate temporally discrete air temperature information but have limited ability to describe its spatial heterogeneity over large areas of the Earth (Benali et al. 2012). Zaksek and Schroedter-Homscheidt (2009) classified the methods used to estimate air temperature based on LST into three approaches: Statistical approaches based on regression techniques, temperature vegetation index and Energy-balance. They have used vegetation index or what is called band ratio for monitoring LST, and indicated that the more built-up areas as obtained from normalized difference building index (NDBI), the more

heat accumulation is taking place. On the other hand, the more vegetation cover as of NDVI the less heat is accumulated.

Sahin, Senkal O, and Pestemalcı (2012) used meteorological and geographical data to develop artificial neural network (ANN) model that estimates LST values in Turkey. Data from 10 meteorological stations during the year 2002 were used for Generalized Regression Neural Network (GRNN) model development. Data of six stations were used for model training, while the remaining data of four stations were utilized for ANN model testing. The model consisted of an input layer with four input parameters, pattern layer, summation layer and output layer with single LST as the output parameter. The researchers concluded that there is a relatively good agreement between the observed and the predicted values of LST, where the RMSE between the estimated and ground values for monthly mean with ANN temperature (in Kelvin) have been found as 0.077 K and 0.091 K (training stations), 0.045 K and 0.003 K (testing stations), respectively.

Kumar, Kumari, and Baskar (2013) have developed ANN model to predict LST from satellite images of land cover/land use (LULC) for Vijayawada city in India. The developed model used NDVI, LULC, Latitude and Longitude in the input layer. Images of the year 2001 were used for model training, while images of the year 2011 were used for model testing. The researchers concluded that the developed ANN model is capable to predict the values of LST with a coefficient of determination (R^2) values of (0.821) and (0.825) for training and testing, respectively. Using microwave remote sensing, an ANN model was developed by Shwetha and Nagesh (2015) to predict LST values under cloudy conditions. In this study LST and MVIs data of the year 2010 for the Cauvery basin in India on a daily basis were obtained from MODIS and advanced microwave scanning radiometer (AMSR-E) sensors of aqua satellite. Results revealed that predictions of LST using ANN are in good agreement with the observed values with the correlation coefficient of 0.846.

Fezizadeh et al. (2013) modelled the spatial variation of LST in Maraqeh Country (Iran) and determined its relationship with LULC. The study found that LST is significantly increasing with urbanization and desertification, as high LST values were found to be associated with rural and urban settlements.

The main objective of this study is to map and simulate the urban LST values in Northern Jordan using remote sensing techniques and artificial neural network modelling.

2. Study area

The study area is located in northern Jordan which extends over four governorates, namely Irbid, Ajloun, Jarash and Mafraq.The coordinates of the studied area are (32° 53.33′36″ N–35°36′E and 32°12.57′34″ N–36°32.98′24″ E) respectively, referenced on the Universal Transverse Mercator system UTM as shown in Figure 2. The total area covered by the study is about 3,941.5 km^2. It has a well-connected roads network with a great variety of geological formations and soil types representing three different climatic and topographic schemes: Highland in Irbid and Ajloun, Desert in Mafraq and Jordan Rift (MWI 2009). In Jordan, rainfall zones can be grouped into three regions, with the highest rainfall (400–600 mm yr^{-1}) occurring in the northwest of the country in upland areas. The second region is far north of the Jordan Valley, lower mean annual rainfall of 250–350 mm occurring in central Jordan.The third region is southern uplands, and the

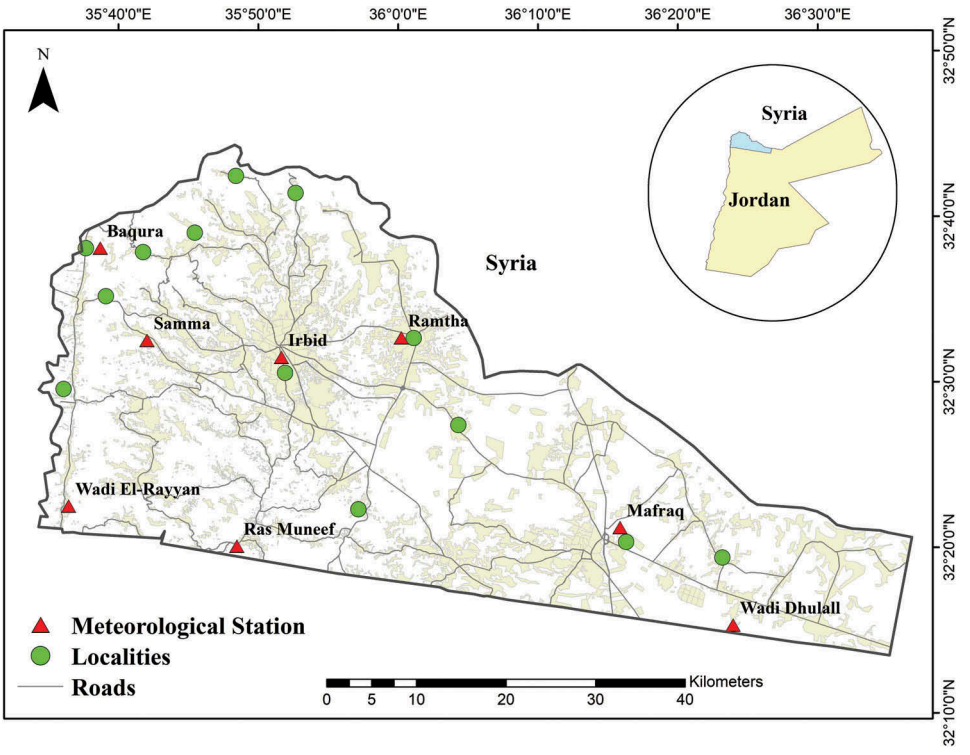

Figure 2. Location of the study area in the north of Jordan.

lowest rainfall (less than 170 mm yr^{-1}) occurring in the lowland regions of the east and south of the country (Freiwan and Kadioglu 2008).

There are eight meteorological stations distributed over the studied area as shown in Figure 2. The meteorological data used in the study included average monthly parameters for the period (1985 to 2016) such as maximum and minimum monthly air temperature, average annual rainfall, and average values of wind velocity, humidity and evaporation. The data used in the study was obtained from the database of the Jordanian Meteorological Department (JMD) and summarized in Table 1.

3. Methodology

To obtain accurate results, the study area was divided into grids with each cell measuring 5 by 5 km. This has resulted in a total of 145 cells. Inside each cell, population and LCLU were expressed in terms of NDVI and NDBI. Furthermore, average air temperature and all other meteorological data were used and correlated with the computed LST for each cell. This procedure was carried out for the whole study period from 2000 to 2016 in both summer and winter seasons. Figure 3 presents a flow chart of the methodology followed in conducting the study.

Table 1. Metrological Parameters of the study area (average annual 1985–2016) (JMD, 2016).

Station	Elevation (m)	Average Annual Rainfall (mm)	Air Temperature (°C) Min	Mean	Max	Relative Humidity (%)	Wind Velocity (km hr^{-1})	Evaporation, Pan (mm)
Irbid	616	485.6	15.8	23.4	18.0	63.8	9.2	195.1
Baqura	−170	375.5	12.6	29.3	22.4	65.2	3.5	195.1
Mafraq	686	126.7	9.5	24.2	16.9	61.1	8.5	195.0
Ramtha	590	288.3	11.2	24.2	18.1	60.7	6.4	190.9
Wadi El-Rayyan	−200	348.6	15.4	30.0	32.2	66.3	1.0	194.9
Samma	332	435.6	15.6	25.7	22.4	63.0	4.6	182.5
Ras Muneef	1150	756.3	10.3	18.8	16.3	68.4	10.1	197.2
Wadi Dhulall	580	116.0	10.3	26.1	17.8	62.4	3.3	195.0

Meteorological data from JMD were fed into a Geographic Information System (GIS) in order to view their spatial distribution over the study area. Interpolation of meteorological data from stations was performed to map these parameters over the whole studied area (Wilson 1990). As an example of this interpolation, Figure 4 shows the distribution of the average annual rainfall computed from the year 1985 to 2016.

Number of Population as an indicator for built-up area expansion is also used to predict LST. Figure 5(a,b) shows the built-up area along with population numbers and their distribution in the study area in the year 2000 (pre-refugee's influxes), while Figure 5(c, d) shows this information for the year 2016 (post-refugees influxes). Comparing these figures, it can be observed that there is a huge expansion in the built-up area, as well as an increase in the number of population and their distribution within the urban and rural centres of the study area.

3.1. *Vegetation indices and built up area*

For the purpose of this research, the atmospheric correction was applied to the satellite images to reduce the noise effect on the acquired satellite images. Normalized Difference Vegetation Index NDVI which is based on the difference between the maximum absorption of radiation in red as a result of chlorophyll pigments and the maximum reflectance in near infra-red (NIR) spectral region as a result of leaf cellular structure was computed using Equation (1) (Tucker 1979):

$$\mathrm{NDVI} = (\rho_{NIR} - \rho_{Red})/(\rho_{NIR} + \rho_{Red}) \tag{1}$$

where ρ_{NIR} is reflectance in the near infra-red band and ρ_{Red} is reflectance in the near red band .The soil spectrum typically does not show such a distinct spectral difference between these bands, and thus the NDVI allows for separation of vegetation from the soil background.

Normalized Difference Built-up Index (NDBI) for the built-up land was developed based on the unique spectral response of built-up lands that have higher reflectance in MIR wavelength range than in NIR wavelength range. Light colours (0 to1) symbolize lands with buildings and dark colours (−1 to 0) symbolize other landscape elements.

The used satellites images in this study along with the acquisition date and satellite sensor are presented in Table 2.

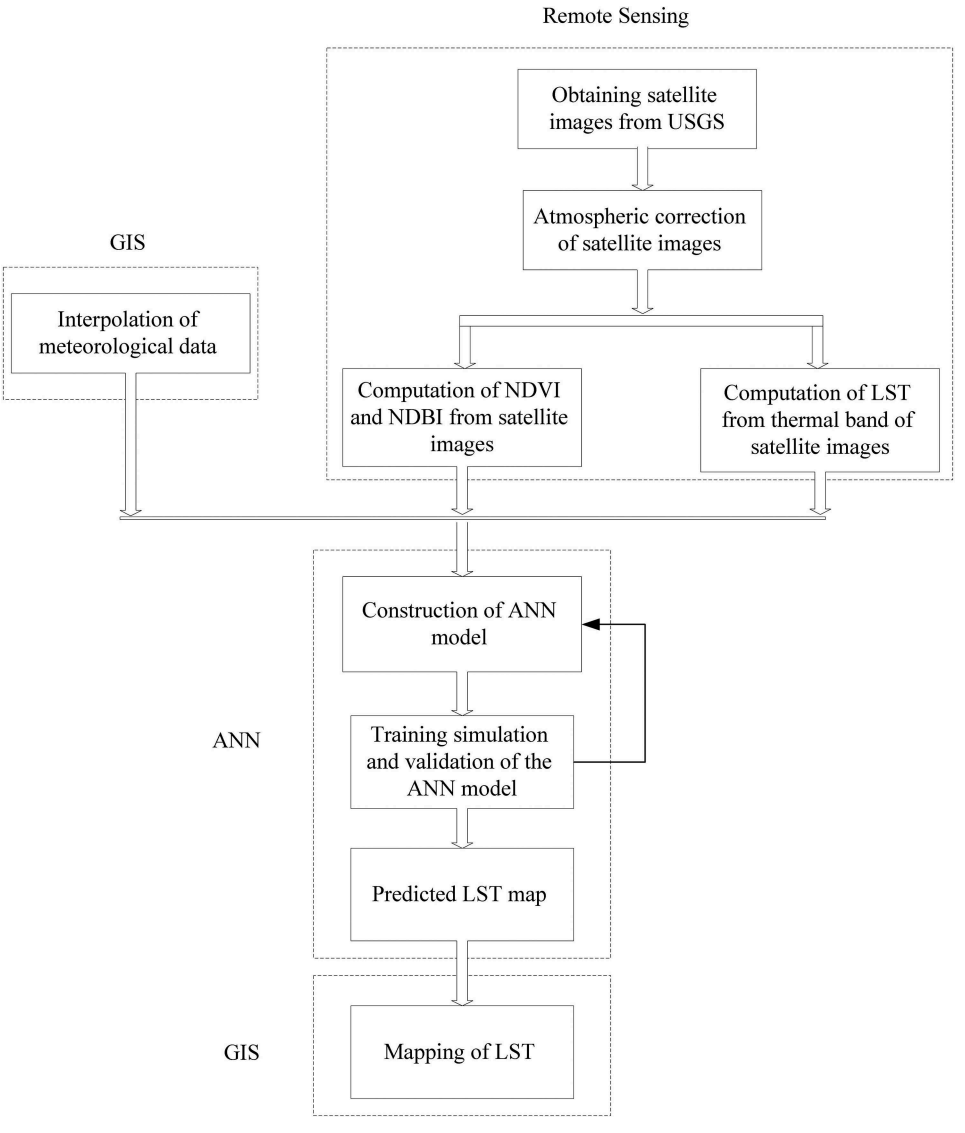

Figure 3. Flow chart showing the methodology followed in conducting the study. (USGS: United States geological survey, LST: Land surface temperature, NDVI: Normalized difference vegetation index, NDBI: Normalized difference building index, GIS: Geographic information system).

Remote sensing data extracted from satellite images were utilized to generate LST values by using Atmospheric correction model (ATCOR) for time series images from the year 2000 to 2016. Two images per year were used to consider the seasonal variations. In Figure 6(a,b), LST thematic maps of summer 2000 and summer 2016 show an increase in LST over the study period. This has enabled to estimate the LST from satellite images without direct measurements in the field which is time-consuming and costly (Jones and Elgy 1994) .

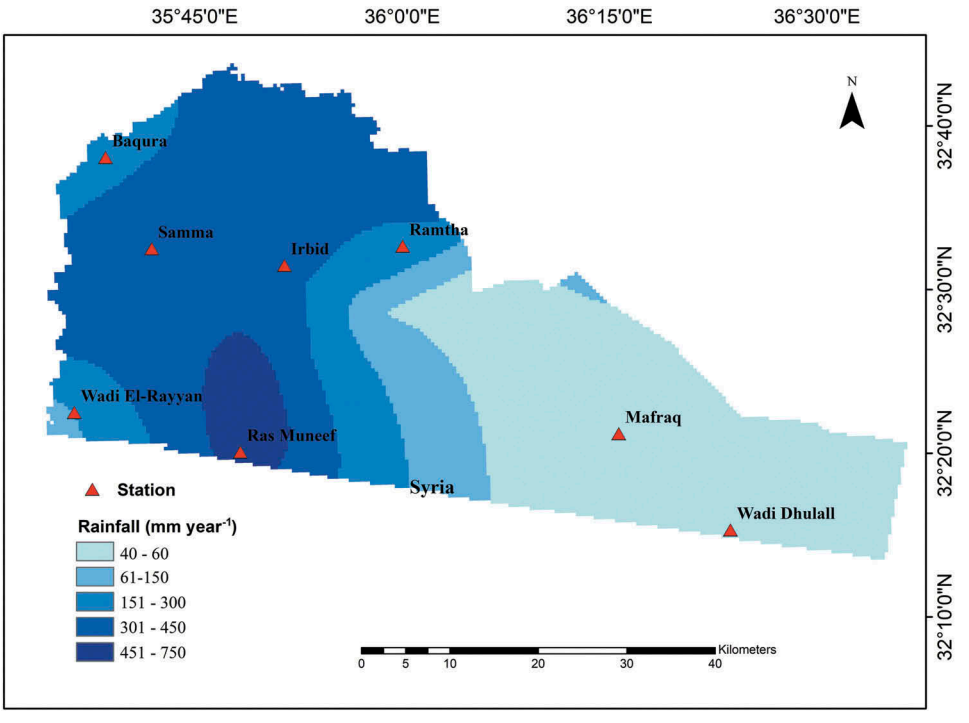

Figure 4. Interpolated average annual rainfall over the studied area for the period 1985–2016.

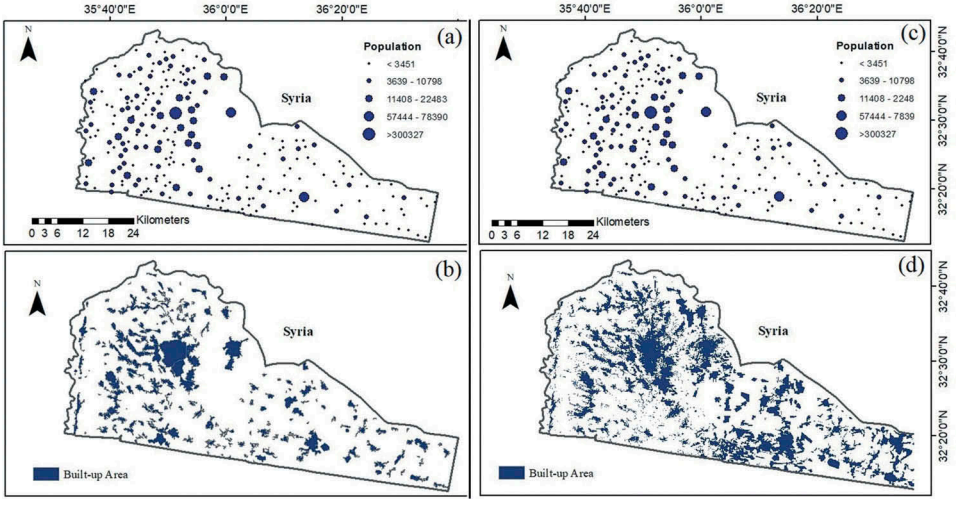

Figure 5. (a). population distribution over the study area in the year 2000, (b). Built-up areas in the year 2000, (c). population distribution over the study area in the year 2016, (d). Built-up areas in the year 2016.

Table 2. LANDSAT satellite images used for computing NDVI, NDBI and LST.

Year	Acquisition Date	Season	Satellite Sensor
2000	7 February 2000	Winter	L-5 TM
2000	14 June 2000	Summer	L-5 TM
2003	13 October 2003	Winter	L-5 TM
2003	9 July 2003	Summer	L-5 TM
2006	5 October 2006	Winter	L-5 TM
2006	30 May 2006	Summer	L-5 TM
2009	30 January 2009	Winter	L-5 TM
2009	23 June 2009	Summer	L-5 TM
2013	27 December 2013	Winter	L-8 OLI
2013	20 July 2013	Summer	L-8 OLI
2015	23 January 2015	Winter	L-8 OLI
2015	8 July 2015	Summer	L-8 OLI
2016	19 February 2015	Winter	L-8 OLI
2016	28 July 2016	Summer	L-8 OLI

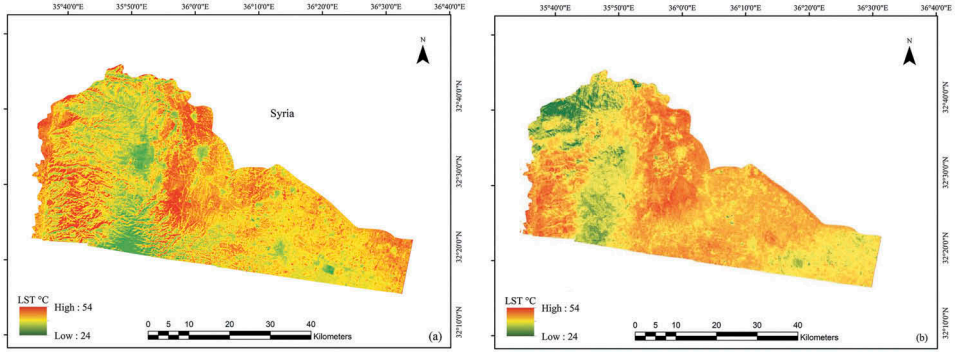

Figure 6. (a). Land surface temperature in northern Jordan, summer 2000. (b). Land surface temperature northern of Jordan, summer 2016.

3.2. *Artificial neural network model*

In order to simulate and predict LST for the next 10 years, ANN is used with nonlinear autoregressive exogenous inputs (NARX) model. NARX is a standard approach for representation of a nonlinear data in discrete time which relates the output y at the discrete time instant t to past outputs and inputs u as shown in Equation (2) (Medsker and Lakhmi 2000).

$$y(t) = f\big(y(t-1), y(t-2), \ldots, y\big(t-n_y\big), u(t-1), u(t-2), \ldots, u(t-n_u)\big) \tag{2}$$

where n_y number of output delays and n_u is the number of input delays. For learning purposes, Levenberg-Marquardt training algorithm (TrainLM) is used for training the network. In order to find the best structure of the network to be used, various network structures were tested and evaluated. The architecture of the selected ANN in the current study is presented in Figure 7 which consists of nine input layers with one hidden layer of eight neurons and one output layer.

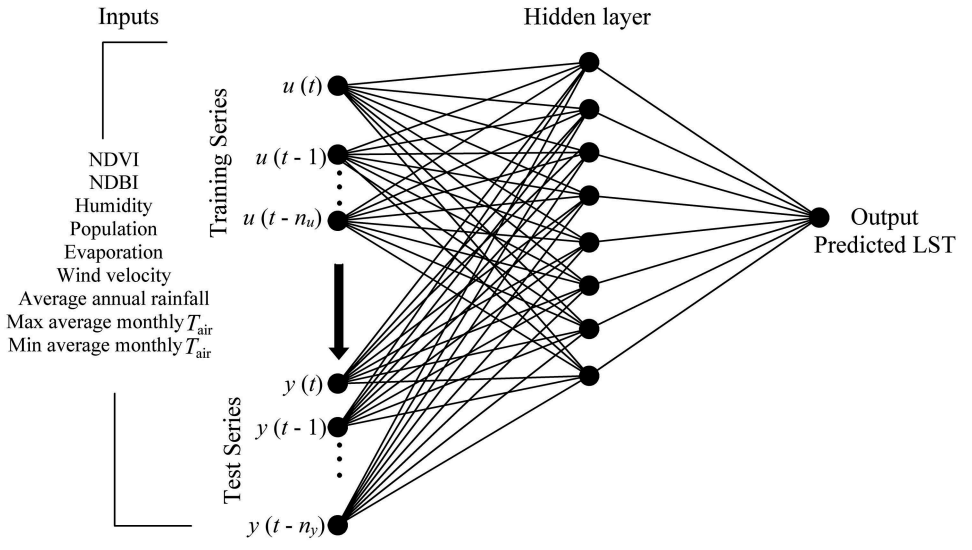

Figure 7. General Architecture of the ANN model used in LST simulation and prediction.

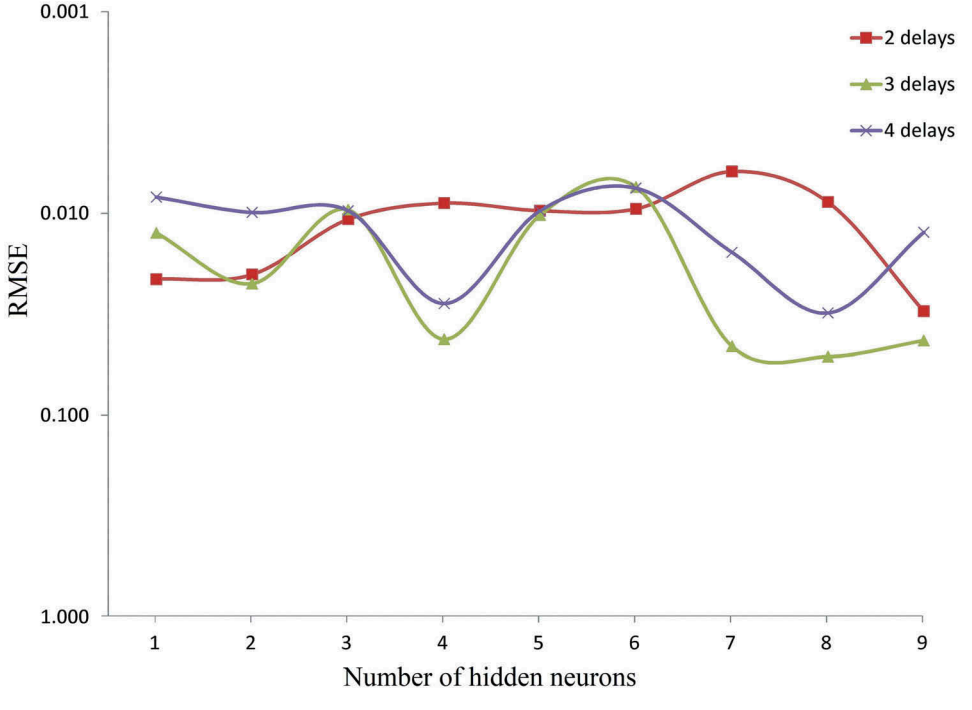

Figure 8. Training trails to find the optimal architecture of the ANN Model.

The total data points used in the model development were 1885 points which represent all cells of the study area. These data points were divided into data set to build the model through the training process (65%), while 15% of the data points were used for model

Table 3. Training trials to find the optimal number of hidden Neurons.

	RMSE		
No. of hidden Neurons	2 Delays	3 Delays	4 Delays
2	0.0212	0.0125	0.0083
3	0.0201	0.0223	0.0099
4	0.0107	0.0096	0.0097
5	0.0089	0.0421	0.0280
6	0.0097	0.0102	0.0097
7	0.0095	0.0074	0.0075
8	0.0062	0.0456	0.0156
9	0.0088	0.0513	0.0312
10	0.0306	0.0427	0.0124

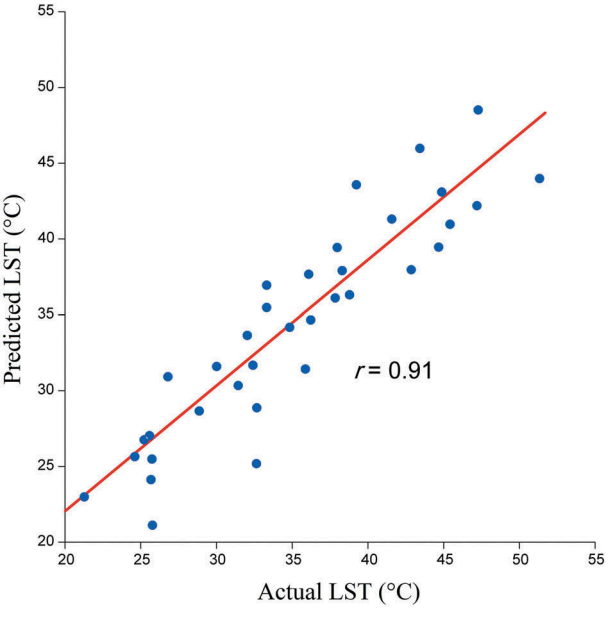

Figure 9. Performance of the ANN model.

validation to measure its performance by holding constant parameters, and finally, 20% of the data points were utilized for model testing to improve its robustness.

4. Results and discussions

Many training trials of the model reviled that using two delays inputs and eight neurons has given the best training results of the ANN as indicated by the low value of the mean squared error of 0.00622. The training trials are presented in Figure 8 and Table 3. The generated ANN model was validated using a set data for another 35 days that were not used in the training of the original model, the relation between the LST data used in the validation process and the predicted values of LST presented in Figure 9.The correlation coefficient – which is a statistical measure that calculates the strength of the relationship between the relative movements of the two variables – was found to be 0.91 for the validation set. Using satellite images and ANN

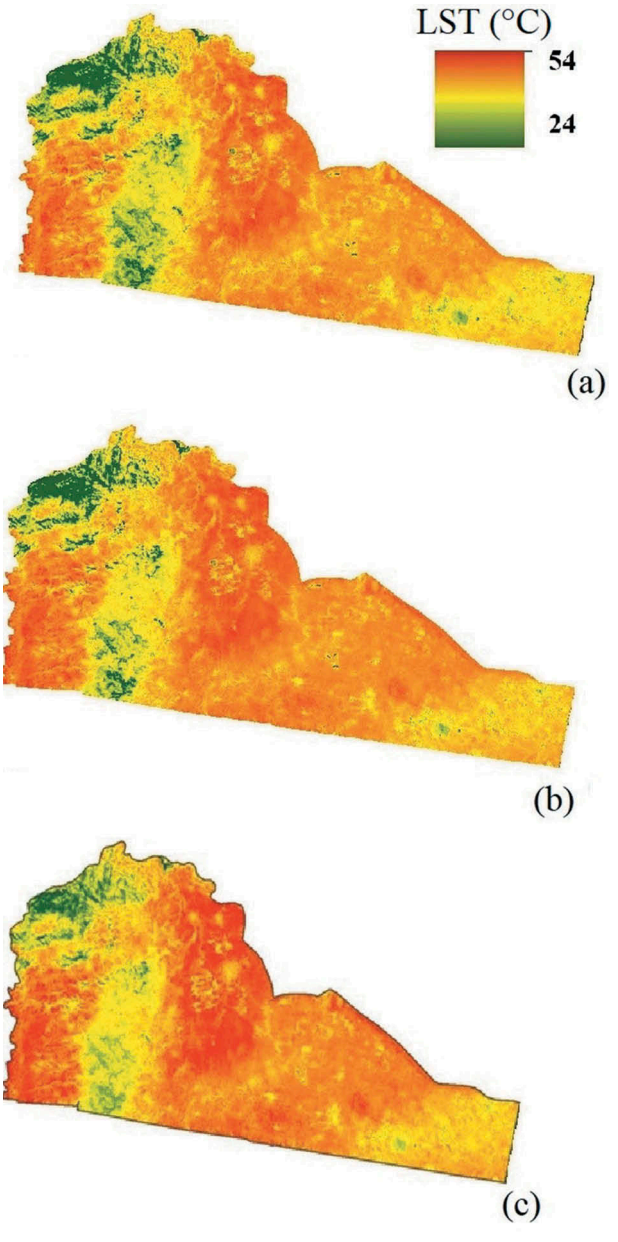

Figure 10. (a). Predicted LST map in 2019, 10 (b). Predicted LST map in 2023, 10 (c). show the predicted LST over the study area in the year 2026.

to predict LST, Maduako et al. (2016) reported a lower value of correlation coefficient ($r = 0.85$). The difference in the values of the correlation coefficients between this study and that of Maduako et al. (2016) may be attributed to the number of satellite images that were used in the studies. In this study, 13 satellite images were used, which covered both summer and winter seasons, while in Madukao et al. (2016) only five images were used to cover a study period of 28 years (1986–2014). The high values of the correlation coefficient indicate that the

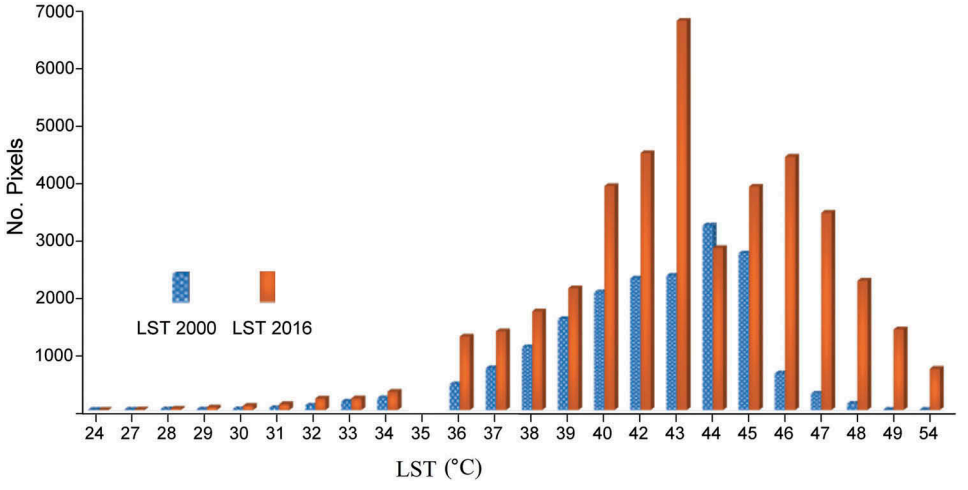

Figure 11. Actual, tested and predicted average values of LST.

developed ANN model is capable to predict the LST with a relatively high level of accuracy by using the mentioned input parameters.

Based on the predicted LST values for the next 10 years, Figure 10(a) shows predicted LST over the study area in the year 2019, while Figure 10(b,c) show the predicted LST over the study area in the years 2023 and 2026 respectively, which represent the beginning, the middle and the end of the period over which the LST was predicted. It can be observed from the three figures that the LST value ranging from as low as 24°C to as high as 54°C. However, the fraction of the study area where LST is getting higher is increasing with time. For example, it can be observed that the LST values are increasing nearby the urban centres that witnessed an expansion and expected to continue expanding (Mushore et al. 2017).

The average estimated increase in LST is 1.1°C as computed from the LST values, this average expected increase in temperature can be considered significant and acceptable with reference to local and international study results, for example: the mean local temperature in Jordan has increased rapidly during the period (1992 to 2008) by 1.5–2 °C. (Matouq et al. 2013). While the IPCC predicts an increase in global mean temperature in the next century by 1°C to 3°C (IPCC 2013).

Figure 11 shows an increasing trend of the generated average LST map for the years 2000 to 2017, the average temperature in the map of the year 2000 is less than that in the year 2016 for most of LST values, as represented in terms of the total number of pixels that have the same LST value.

5. Conclusions

Expansion of urban areas usually contributes to the creation of urban heat islands and consequently increases in the magnitude of LST. This is especially true for Jordan which has witnessed during the last two decades several refugees' influxes that resulted in changes of the LCLU characterized by the expansion of built-up areas. Remote sensing data have been widely

used in deriving the values of LST. In this study, ANN model was developed to predict LST based on the meteorological data and LCLU that acquired from satellite images of Northern Jordan. The developed ANN model is capable to simulate and predict LST of the study area with a reasonable accuracy as judged by high values of correlation coefficient and low value of RMSE. Thus, with the current trend, if the LCLU continues, the level of LST in the study area is expected to be increased further. The average predicted value of increase by the end of the study period (year 2026) is 1.1°C. The methodology adopted in this study by combining remote sensing techniques and meteorological data in developing the ANN model is an effective one for predicting LST in arid to semi-arid areas like Northern Jordan.

It is recommended that future research should cover the variation of LST value considering seasonality between summer and winter.

Disclosure statement

No potential conflict of interest was reported by the authors.

ORCID

Nawras Shatnawi http://orcid.org/0000-0001-6752-1810

References

Ahmed, B., K. M, X. Zhu, S. Rahman, and K. Choi. 2013. "Simulating Land Cover Changes and Their Impacts on Land Surface Temperature in Dhaka, Bangladesh." *Remote Sensing* 5: 5969–5998.

Al-Seroury, F. A. 2012. "Temporal Changes of Air Pollutants and Land Surface Temperature around Jeddah Desalination Power Plant, K S A." *Journal of American Science* 8 (2): 503–508.

Asimakopoulos, D. N., V. D. Assimakopoulos, and N. Chrisomallidou. 2001. *Energy and Climate in the Urban Built Environment*. London, UK: James & James Publication.

Avelar, S., R. Zah, and C. Tavares-Corrêa. 2009. "Linking Socioeconomic Classes and Land Cover Data in Lima, Peru: Assessment through the Application of Remote Sensing and GIS." *International Journal of Applied Earth Observation and Geoinformation* 11: 27–37. doi:10.1016/j.jag.2008.05.001.

Benali, A., A. C. Carvalho, J. P. Nunes, N. Carvalhais, and A. Santos. 2012. "Estimating Air Surface Temperature in Portugal Using MODIS LST Data." *Remote Sensing of Environment* 124: 108–121. doi:10.1016/j.rse.2012.04.024.

Bhargava, A., S. Lakmini, and S. Bhargava. 2017. "Urban Heat Island Effect: It's Relevance in Urban Planning." *Journal of Biodiversity and Endanger Species* 5: 2.

Chow, V. T., D. R. Maidment, and L. W. Mays. 1988. *Applied Hydrology*. Singapore: McGraw-Hill.

DOS (Jordan Department of Statistics). 2017 "Final Results of the 2017 Population and Housing Census." Accessed 23 Aug 2018. http://dosweb.dos.gov.jo/censuses/population-and-housing/population-and-housing-2017/

Emmanuel, M. R. 2005. *An Urban Approach to Climate-Sensitive Design; Strategies for the Tropics*. London, UK: Spon Press.

Fezizadeh, B., T. Blaschke, H. Nazmfar, E. Akbari, and R. Kohbanani. 2013. "Monitoring Land Surface Temperature Relationship to Land Use/Land Cover from Satellite Imagery in Maraqeh County." *Iran, Journal of Environmental Planning and Management* 56: 1290–1315. doi:10.1080/09640568.2012.717888.

Freiwan, M., and M. Kadioglu. 2008. "Spatial and Temporal Analysis of Climatological Data in Jordan." *International Journal of Climatology* 28 (4): 521–535. doi:10.1002/(ISSN)1097-0088.

Hadadin, N. A., and Z. S. Tarawneh. 2007. "Environmental Issues in Jordan." *Solutions and Recommendations, American Journal of Environmental Sciences* 3 (1): 30–36.

IPCC. 2013. "Summary for Policymakers." In *Climate Change 2013: The Physical Science Basis. Contribution of Working Group I to the Fifth Assessment Report of the Intergovernmental Panel on Climate Change*, edited by T. F. Stocker, D. Qin, G.-K. Plattner, M. Tignor, S. K. Allen, J. Boschung, A. Nauels, Y. Xia, V. Bex, and P. M. Midgley. Cambridge, United Kingdom and New York, NY, USA: Cambridge University Press, 3–27.

JMD. 2016. Jordan Annual Climate Bulletin. Amman: Jordan Meteorological Department.

Jones, H. K., and J. Elgy. 1994. "Remote Sensing to Assess Landfill Gas Migration." *Waste Management and Research* 12: 327–337. doi:10.1177/0734242X9401200405.

Kaya, S., U. G. Basar, M. Karaca, and D. Z. Seker. 2012. "Assessment of Urban Heat Islands Using Remotely Sensed Data." *Ekoloji* 21 (84): 107–113. doi:10.5053/ekoloji.

Kuhn, K., D. Campbell-Lendrum, and C. Davies. 2002. "A Continental Risk Map for Malaria Mosquito (Diptera: Culicidae) Vectors in Europe." *Journal of Medical Entomology* 39 (4): 621–630.

Kumar, K. S., K. P. Kumari, and P. U. Baskar. 2013. "Artificial Neural Network Model for Prediction of Land Surface Temperature from Land Use/Cover Images." *International Journal of Advanced Trends in Computer Sciebce and Engineering* 2: 87–92.

Li, Z. L., and F. Becker. 1993. "Feasibility of Land Surface Temperature and Emissivity Determination from AVHRR Data." *Remote Sensing of Environment* 43: 67–85. doi:10.1016/0034-4257(93)90065-6.

Maduako, ID., Z. Yun, and B. Patrick. 2016. "Simulation and Prediction of Land Surface Temperature (LST) Dynamics within Ikom City in Nigeria Using Artificial Neural Network (ANN)." *Journal of Remote Sensing and GIS,* 5 (1): 1–7.

Makhamreha, Z., and N. Almanasyeha. 2011. "Analyzing the State and Pattern of Urban Growth and City Planning in Amman Using Satellite Images and GIS." *European Journal of Social Sciences* 24: 252–264.

Matouq, M., T. El-Hasan, H. Al-Bilbisi, M. Abdelhadi, M. Hindiyeh, S. Eslamian, and S. Duheisat. 2013. "The Climate Change Impaction on Jordan: A Case Study Using GIS and Artificial Neural Networks for Weather Forecasting." *Journal of Taibah University for Science* 7 (1): 44–55. doi:10.1016/j.jtusci.2013.04.001.

Medsker, L., and J. Lakhmi. 2000. *Recurrent Neural Networks: Design and Applications*. Boca Raton,. FL: CRC press.

Mushore, T. D., O. Mutanga, J. Odindi, and T. Dube. 2017. "Linking Major Shifts in Land Surface Temperatures to Long Term Land Use and Land Cover Changes: A Case of Harare." *Zimbabwe, Urban Climate* 20: 120–134. doi:10.1016/j.uclim.2017.04.005.

MWI. 2009. "Ministry of Water and Irrigation." *Annual report of water authority of Jordan*. Amman, Jordan.

Oke, T. R., G. T. Johnson, D. G. Steyn, and I. D. Watson. 1991. "Simulation of Surface Urban Heat Islands under Ideal Conditions at Night—Part 2: Diagnosis of Causation." *Boundary-Layer Meteorology* 56 (4): 339–358. doi:10.1007/BF00119211.

Prince, S. D., and S. N. Goward. 1995. "Global Primary Production: A Remote Sensing Approach." *Journal of Biogeography* 22: 815–835. doi:10.2307/2845983.

Sahin, M., Y. Y. Senkal O, and V. Pestemalcı. 2012. "Modelling and Remote Sensing of Land Surface Temperature in Turkey." *Journal of Indian Society of Remote Sensing* 40: 399–409. doi:10.1007/s12524-011-0158-3.

Shahmohamadi, P. A., I. A. Che-Ani, A. Ramly, K. N. A. Maulud, and M. F. I. Mohd-Nor. 2010. "Reducing Urban Heat Island Effects: A Systematic Review to Achieve Energy Consumption Balance." *International Journal of Physical Sciences* 5 (6): 626–636.

Shwetha, H. R., and K. Nagesh. 2015. "Prediction of Land Surface Temperature under Cloudy Conditions Using Microwave Remote Sensing and ANN." *Aquatic Procidia* 4: 1381–1388. doi:10.1016/j.aqpro.2015.02.179.

Tucker, C. J. 1979. "Red and Photographic Infrared Linear Combinations for Monitoring Vegetation." *Remote Sensing of Environment* 8: 127–150. doi:10.1016/0034-4257(79)90013-0.

UN-Habitat. 2016. *Urbanization and Development: Emerging Futures, World Cities Report*. Nairobi, Kenya: United Nations Human Settlements Program (UN-Habitat).

UNHCR. 2014. "Syria Regional Refugee Response." UNHCR. http://data.unhcr.org/syrianrefugees/country.php?id=107.

UNHCR. (2017). Syrian Refugees in Jordan (Total Population) - District Level as of 31 December 2016, 23 January 2017. Accessed 10 March 2017. http://www.refworld.org/docid/5899d7284.html [accessed 10 March 2017]

Voogt, J. A., and T. R. Oke. 2003. "Thermal Remote Sensing of Urban Climates." *Remote Sensing of Environment* 86: 370–384. doi:10.1016/S0034-4257(03)00079-8.

Weber, C. 2001. "Urban Agglomeration Delimitation Using Remote Sensing Data. In *Remote Sensing and Urban Analysis*, edited by Donnay J. P., Barnsley M. J. and Longley P. A. London and New York: Taylor and Francis, 155–167.

Wilson, E. M. 1990. *Engineering Hydrology*. 4th ed. UK: English language book society/Macmillan education .

World Bank. 2017. "Cities of Refuge in the Middle East: Bringing an Urban Lens to the Forced Displacement Challenge." *Policy Note September* 14: 7.

Zaksek, K., and M. Schroedter-Homscheidt. 2009. "Parameterization of Air Temperature in High Temporal and Spatial Resolution from a Combination of the SEVIRI and MODIS Instruments." *ISPRS Journal of Photogrammetry and Remote Sensing* 64 (4): 414–421. doi:10.1016/j.isprsjprs.2009.02.006.

Zhang, Z., M. Ji, J. Shu, Z. Deng, and Y. Wu. 2008. "Surface Urban Heat Island in Shanghai, China: Examining the Relationship between Land Surface Temperature and Impervious Surface Fractions Derived from Landsat ETM+ Imagery." *The International Archives of the Photogrammetry, Remote Sensing and Spatial Information Sciences* 37: 601–606.

Zheng, S., X. Zhou, R. Singh, Y. Wu, Y. Ye, and C. Wu. 2017. "The Spatiotemporal Distribution of Air Pollutants and Their Relationship with Land-Use Patterns in Hangzhou City, China." *Atmosphere* 8: 110. doi:10.3390/atmos8060110.